Article ID: 1000-324X(2014)10-1115-06 **DOI:** 10.15541/jim20140104

Morphology Evolution in Hydrothermal Synthesis of Mesoporous Alumina

LI Yan-Hui, PENG Cheng, ZHAO Wei, BAI Ming-Min, RAO Ping-Gen

(School of Materials Science and Engineering, South China University of Technology, Guangzhou 510640, China)

Abstract: Boehmite with varied morphologies was successfully synthesized from aluminum ammonium sulfate hydrate and urea, as well as poly-glycol-2000 by hydrothermal method. The experimental results show that boehmite microspheres, microfibers and 3D hierarchical structured AlOOH can be fabricated only by adjusting hydrothermal temperature. SEM images indicate that boehmite decomposes into γ-Al_2O_3 phase after heat-treatment through a topotactical process. TEM studies present that the mesopores are formed in γ-Al_2O_3 particles. Based on these investigations, a temperature-dependent morphology formation mechanism is proposed. Besides, the as-synthesized alumina excited at 325 nm shows emission in the range of 380 nm to 500 nm, centered at 409 nm and 467 nm.

Key words: boehmite, γ-Al_2O_3; topotactical; mesoporous; photoluminescence

Recently, researches on morphology and structure-dependent properties of inorganic oxides have attracted much attention. As a fascinating kind of functional materials, mesoporous materials have been widely studied due to their applications including catalysts[1-3], sensors[4-5], and magnetic storage of media data[6-7]. Many mesoporous structured oxides such as α-MoO_3[8], SiO_2[9], TiO_2[10] and Al_2O_3 have been fabricated successfully in the past years. Especially, Al_2O_3 has been extensively investigated owing to its distinct physical and chemical properties, such as thermal stability and acid-base amphoteric character. However, researches on the formation mechanism alumina with mesoporous structure are still limited.

Conventionally, mesoporous alumina can be prepared by template method, including soft template of surfactants[11-12], amphiphilic polymer[13-14], and hard template of mesoporous silica[15-16], carbon[17-18]. Recently, some other methods have been employed to synthesis mesoporous alumina, such as evaporation-induced method[19], Sol-Gel method[20] and multi-component method[21]. However, a general strategy for the synthesis of alumina with controlled morphology and porous structure is still beyond the scope of current implementation.

In this work, we introduced a simple hydrothermal method to fabricate boehmite (AlOOH) with three different morphologies in the presence of surfactant poly-glycol (PEG)-2000. Mesoporous structured γ-Al_2O_3 was prepared by decomposition of the as-produced AlOOH. Besides, the growth mechanism of AlOOH and the mesoporous structure of γ-Al_2O_3 were studied, and photoluminescence (PL) of the as-synthesized alumina was also investigated.

1 Experiments

All chemicals were used without further purification. γ-Al_2O_3 with various morphologies was prepared as follows. First, 9.07 g $NH_4Al(SO_4)_2{\cdot}12H_2O$, 0.2 g (PEG)-2000 and 15 g urea were dissolved into 100 mL deionized water under vigorously stirring till a transparent solution was formed. And then, the resulting solution was sealed in the 250 mL Teflon-lined stainless steel autoclave, and was placed in oven at different hydrothermal temperatures for 12 h. Finally, the precipitation was collected by centrifugation, washed with deionized water and ethanol for 4 times, and dried at 80℃. γ-Al_2O_3 was obtained by calcination of the collected precursors at 800℃ for 2 h with a heating rate of 10 ℃/min. The hydrothermal products synthesized at 90℃, 120℃ and 150 ℃ were named as Pre90, Pre120 and Pre150, respectively. Correspondingly, their calcined products were denoted as Alu90, Alu120 and Alu150.

X-ray diffraction (XRD, PANalytical X'Pert PRO, Almelo, Holland) and scanning electron microscope (SEM, ZEISS EVO 18, Oberkochen, Germany) were used to study the crystallinity and morphology of prepared powders, respectively. The mesoporous microscopic features of the as-obtained γ-Al_2O_3 were characterized using a transmission electron microscope (TEM, JEM-2100, Tokyo, Japan). Average mesopore size distribution was

Received date: 2014-03-07; **Modified date:** 2014-06-23; **Published online:** 2014-07-20
Foundation item: Science and Technology Program of Guangdong Province of China(2012B091000107)
Biography: LI Yan-Hui(1986–), female, candidate of PhD. E-mail: lyhklyg@163.com
Corresponding author: RAO Ping-Gen, professor. E-mail: pgrao@scut.edu.cn

measured by Barrett-Joyner-Halenda (BJH, Micromeritics ASAP2020, Atlanta, America) method from the desorption branch of isotherm. Photoluminescence analyses were performed with Jobin-Yvon Triax 320 spectrometer (PL, Jobin-Yvon Triax 320, Paris, France).

2 Results and discussion

Figure 1(A) shows the typical XRD patterns of AlOOH prepared at 90℃, 120℃ and 150℃ for 12 h. XRD pattern of Pre90 in Fig. 1(A) presents that the as-obtained powder is amorphous, while the patterns of Pre120 and Pre150 can be readily indexed to the crystalline phase of AlOOH (JCPDS 01-072-0359). XRD patterns of Fig. 1(A) indicate that the hydrothermal temperature favors the particle's crystallization. Generally, the crystal growth is determined by the rate of crystal formation and migration, which are influenced by the temperature. The lower temperature leads to the lower growth rate of crystals[22]. Figure 1(B) presents the XRD patterns of the samples obtained by calcinations of AlOOH at 800℃ for 2 h. All the diffraction peaks can be identified as cubic γ-Al_2O_3 (JCPDS 00-001-1303). Figure 1(C) shows the small-angle XRD patterns of γ-Al_2O_3. The products show a strong diffraction peak at around 0.3º, indicating that the mesoporous structure exists in these samples.

Figure 2 exhibits the different magnification SEM images of the as-obtained AlOOH. It shows that the sphere-like particle with non-uniform size is synthesized at 90℃ for 12 h in Fig. 2(A-B). The diameter of the sphere ranges from 1–5 μm and its surface is apparently smooth. Figure 2(C) and (D) show the SEM images of-Pre120 which is composed of uniform and straight fibers with the length of 10–20 μm and the diameter of 200–500 nm. As the hydrothermal temperature increases to 150℃, a large number of flower-like particles with hierarchical structure are formed(Fig. 2(E-F)). The diameter of the flowers is 3–5 μm. Every flowers comprises numerous microfibers with length of 1–3 μm and a diameter of 20–30 nm, as shown in Fig. 2(E) and (F). The SEM results reveal that the hydrothermal temperature has an obvious effect on the morphology of the as-prepared precursor.

Figure 3 shows the SEM images of γ-Al_2O_3 obtained by calcinations of the precursors. These samples show similar morphology to that of precursors. These results indicate that the transformation from AlOOH to cubic γ-Al_2O_3 without obvious morphology change and volume shrinkage, is known as a topotactical process[23-24]. The crystal tructure of AlOOH is orthorhombic, space group Amam (NO. 63) with a=0.369 nm, b=1.224 nm, c=0.286 nm, $\alpha=\beta=\gamma$=90°, Z=4. The crystal structure of γ-Al_2O_3 is cubic, space group Fd-3m (NO. 227) with $a=b=c$= 0.79 nm, $\alpha=\beta=\gamma$= 90°, Z=10. Comparing both above crystal structure, the transformation from AlOOH to γ-Al_2O_3 is involves only the vibration of corresponding axes other than change of the angle shift, which provides a basis for topotactical transformation[25].

In order to observe the details of morphological structure of γ-Al_2O_3, the high-resolution transmission electron microscopy (TEM) is employed. Figure 4(A-B) present the TEM images and SAED patterns (inset) of Alu90. γ-Al_2O_3 solid sphere with non-uniform diameter can be observed from Fig. 4(A), and Fig. 4(B) presents the microsphere is assembled by small particles. The TEM images and SAED patterns (inset) of Alu120 (Fig. 4(C-D)) clearly display that γ-Al_2O_3 microfibers are prepared and the mesopores are formed homogenously in the fibers. Figure 4(E-F) show the TEM images and SAED patterns (inset) of Alu150. It is observed that the fiber-like blocks are composed of small crystals with mesopores of pore size less than 20 nm. The SAED patterns in Fig. 4 show that all the crystal phases of the products are polycrystalline. The TEM results present that γ-Al_2O_3 is consisted of small crystals and the mesopores structure is formed by decomposition of AlOOH and PEG 2000, which is consistent with SEM results.

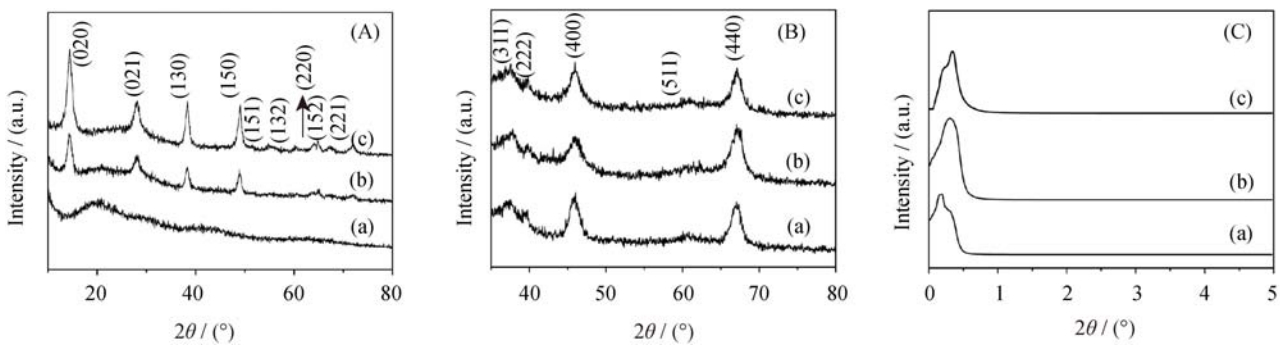

Fig. 1 XRD patterns of AlOOH (A), together with their respective (B) wide- and (C) small-angle XRD patterns of γ-Al_2O_3 powder calcined at 800℃ for 2 h

(a) Pre90; (b) Pre120; (c) Pre150

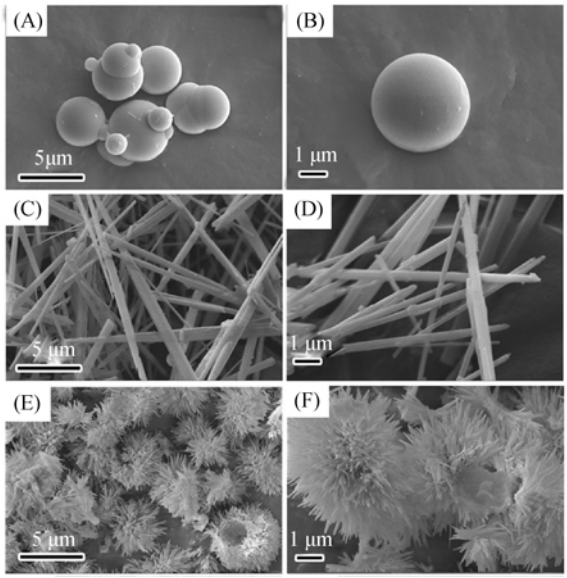

Fig. 2 SEM images of AlOOH
(A-B)Pre90;(C-D)Pre120;(E-F)Pre150

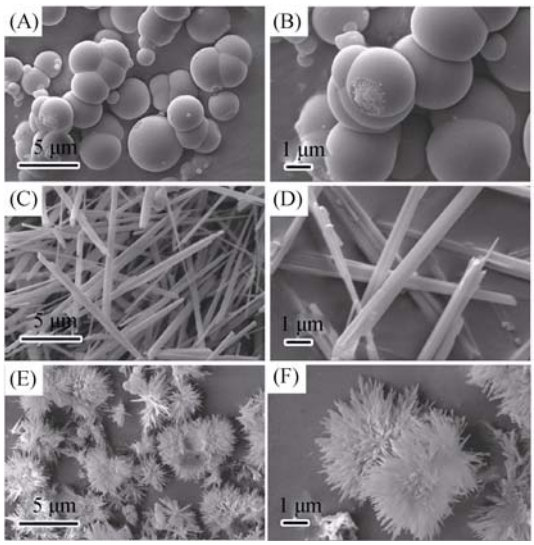

Fig. 3 SEM images of γ-Al_2O_3 obtained from different hydrothermal products calcined at 800℃ for 2 h
(A-B) Alu90; (C-D) Alu120; (E-F) Alu150

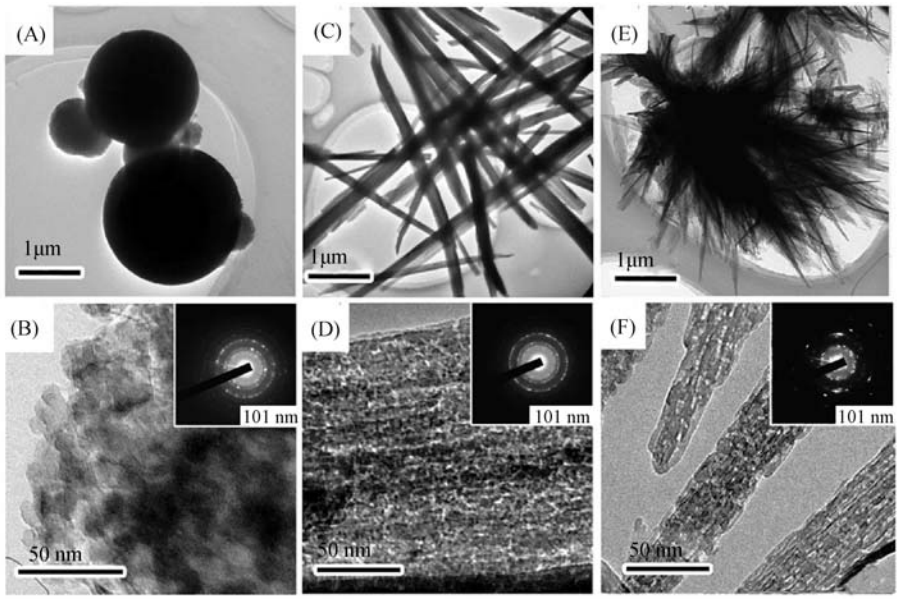

Fig. 4 TEM image and a typical SAED pattern (inset) of γ-Al_2O_3
(A-B) Alu90; (C-D) Alu120; (E-F) Alu150

Figure 5 presents the BJH pore-size distribution and N_2adsorption-desorption isotherm of γ-Al_2O_3 obtained by calcination of the precursors at 800℃. The pore size distribution curves of γ-Al_2O_3 in Fig. 5(A-B) exhibit that they have the same sized mesopores, while the pore size distribution of Alu150 (Fig. 5(C)) centers at 13 nm and 250 nm. The corresponding N_2 absorption-desorption isotherm curves in Fig. 5(D-F) are IV type with the pressure range of P/P_0 at 0.4–0.9, 0.4–1.0 and 0.7–1.0, respectively. The curves of Fig. 5(D-E) with a hysteresis of H1 present that there exists mesopores, while the curve of Fig. 5(F) with an H4 hysteresis loop indicates that there exists silted pores due to the center cores in 3D structure. Meanwhile, the BET surface areas of the as-obtained powders are 125, 105 and 101 m^2/g, and Langmuir surface areas are 173, 148 and 140 m^2/g, respectively. The mesoporous structure of these products is beneficial to the potential applications in catalyst material.

Based on the above results, we propose a formation mechanism of different shaped γ-Al_2O_3, as presented in Fig. 6. The growth of AlOOH is composed of the process of precipitation from supersaturated solution and ostwald ripening. Urea hydrolyzes under hydrothermal conditions and boehmite precursor can be formed by the following reactions[26]:

$$CO(NH_2)_2 + H_2O \rightarrow CO_2\uparrow + 2NH_3 \quad (1)$$

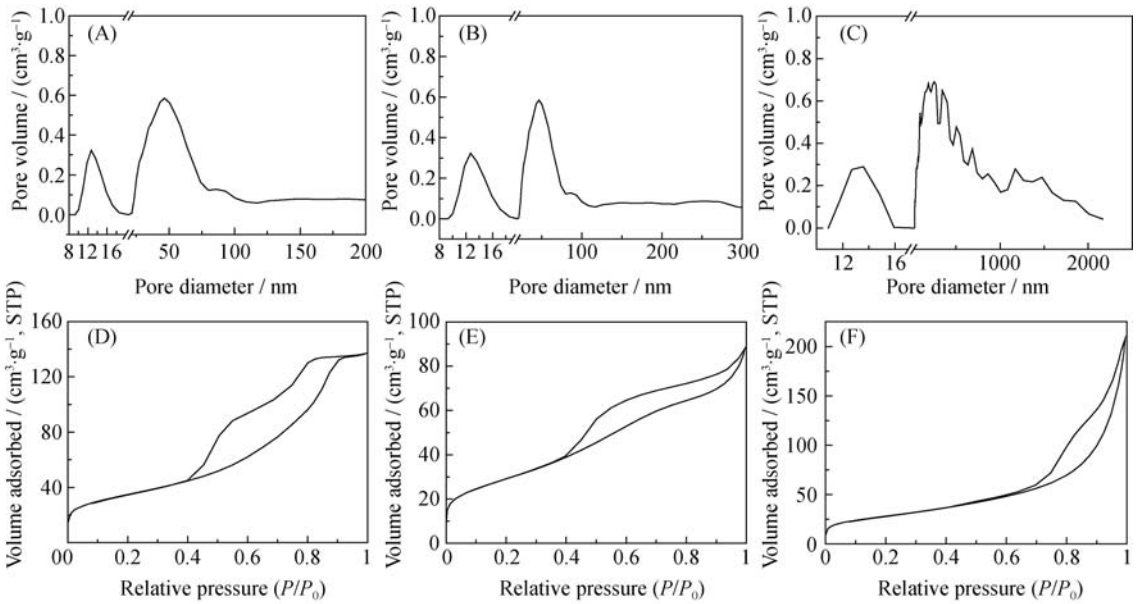

Fig. 5 Barrett-Joyner-Halenda (BJH) pore-size distribution (A-C) and N_2 adsorption and desorption isotherm (D-F) of γ-Al_2O_3 from different hydrothermal products

(A, D) Alu90; (B, E) Alu120; (C, F) Alu150

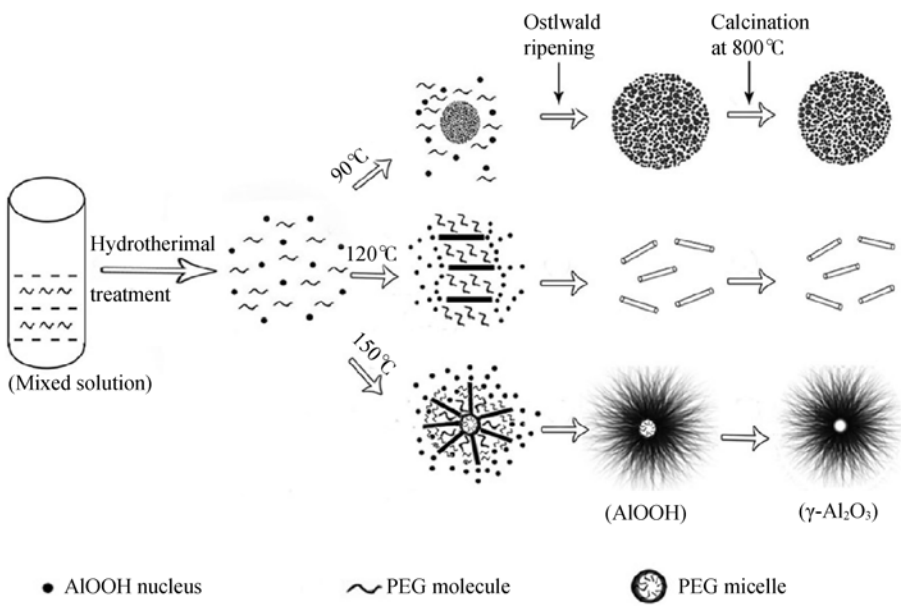

Fig. 6 Schematic diagram of the formation of AlOOH precursor with various morphologies

$$NH_3 + H_2O \rightarrow NH_4^+ + OH^- \quad (2)$$

$$Al^{3+} + 3OH^- \rightarrow AlOOH + H_2O \quad (3)$$

At the initial of the hydrothermal process, AlOOH is formed due to the hydrolysis of urea, which is based on the mechanism of precipitation from supersaturated solution[27]. When the hydrothermal temperature is kept at 90℃, the energy is not enough for crystal orientation, leading to the low growth rate of every crystal plane, and microsphere[28]. As the temperature increases to 120℃, the crystal plane with grows preferentially, driven in part by relatively high surface energy and in part by a kinetic effect involving a cyclic generation of highly reactive adsorption sites[29]. Eventually, AlOOH microfibers are fabricated. At 150℃, initially, the PEG micelle is formed due to the higher temperature resulting in the lower critical micelle concentration[30-31]. Then the AlOOH microfibers attach onto the PEG micelle, and the flower-like hierarchical structured AlOOH is formed[32]. After calcination at 800℃, γ-Al_2O_3 is obtained with the morphology and volume of AlOOH remained according to Eq. (4), known as topotactical process.

$$2AlOOH \rightarrow Al_2O_3 + H_2O \quad (4)$$

Figure 7 shows the PL spectrum of micrometer-sized γ-Al_2O_3 with mesoporous structure. The PL spectra present that absorption and emission bands show almostno change with the crystal size and morphology, illustrating that the emission bands are attributed only to color centers. The spectrum is composed of a broad band, a strong peak

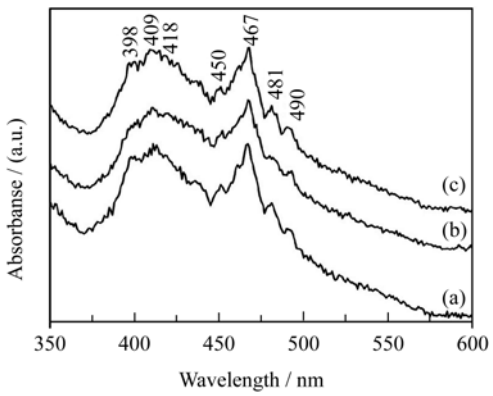

Fig. 7　Room temperature PL spectra of the as-prepared γ-Al_2O_3 (a) Alu90; (b) Alu120; (c) Alu150

located at 467 nm from emission of Xenon lamp and several weak peaks with excitation 325 nm. The broad band is consisted of three peaks at 398, 409 and 418 nm, ascribed to F centers, and the strong peak is at 467 nm with several shoulders at around 450, 481 and 490 nm, which are ascribed to the P centers[12, 33].

3　Conclusions

AlOOH microspheres, microfibers and 3D hierarchical structure can be synthesized at hydrothermal temperature of 90℃, 120℃ and 150℃, respectively. After calcination, γ-Al_2O_3 with similar morphologies with AlOOH precursors is formed through a topotactical thermal decomposition process. Owing to this formation process, the prepared γ-Al_2O_3 shows mesoporous properties and has large surface area, which might be useful for their potential application in catalyst. Besides, the PL results present that the as-synthesized γ-Al_2O_3 exhibits strong emission at room temperature.

References:

[1] UDDIN A, TSUDA H, WU S, *et al*. Catalytic decomposition of biomass tars with iron oxide catalysts. *Fuel*, 2008, **87(4):** 451–459.

[2] ZHU Z, LIU H, SUN H, *et al*. Surfactant assisted hydrothermal and thermal decomposition synthesis of alumina microfibers with mesoporous structure. *Chem. Eng. J.*, 2009, **155(3):** 925–930.

[3] PHAM A L T, LEE C, DOYLE F M, *et al*. A silica-supported iron oxide catalyst capable of activating hydrogen peroxide at neutral pH values. *Environ. Sci. Technol.*, 2009, **43(23):** 8930–8935.

[4] REDDY C, CAO S A W, TAN O, *et al*. Preparation and Characterization of Iron Oxide-zirconia Nano Powder for Its Use as an Ethanol Sensor Material. Ceramics Transactions: Wiley-American Ceramic Society, 2012**:** 67.

[5] BISWAL R C. Pure and Pt-loaded gamma iron oxide as sensor for detection of sub ppm level of acetone. *Sens Actuators B*, 2011, **157(1):** 183–188.

[6] GUARDIA P, LABARTA A, BATLLE X. Tuning the size, the shape, and the magnetic properties of iron oxide nanoparticles. *J. Phys. Chem. C*, 2010, **115(2):** 390–396.

[7] LAURENT S, FORGE D, PORT M, *et al*. Magnetic iron oxide nanoparticles: synthesis, stabilization, vectorization, physicochemical characterizations, and biological applications. *Chem. Rev.*, 2008, **108(6):** 2064.

[8] BREZESINSKI T, WANG J, TOLBERT SH, *et al*. Ordered mesoporous α-MoO_3 with iso-oriented nanocrystalline walls for thin-film pseudocapacitors. *Nat. Mater.*, 2010, **9(2):** 146–151.

[9] VIVERO-ESCOTO J L, SLOWING I I, TREWYN B G, *et al*. Mesoporous silica nanoparticles for intracellular controlled drug delivery. *Small*, 2010, **6(18):** 1952–1967.

[10] CHEN D, HUANG F, CHENG Y B, *et al*. Mesoporous anatase TiO_2 beads with high surface areas and controllable pore sizes: a superior candidate for high-performance dye-sensitized solar cells. *Adv. Mater.*, 2009, **21(21):** 2206–2210.

[11] ROSSINYOL E, ARBIOL J, PEIRÓ F, *et al*. Nanostructured metal oxides synthesized by hard template method for gas sensing applications. *Sens. Actuators B*, 2005, **109(1):** 57–63.

[12] ZHU Z, LIU H, SUN H, *et al*. PEG-directed hydrothermal synthesis of multilayered alumina microfibers with mesoporous structures. *Microporous Mesoporous Mater.*, 2009, **123(1/2/3):** 39–44.

[13] PELLEGRINO T, MANNA L, KUDERA S, *et al*. Hydrophobic nanocrystals coated with an amphiphilic polymer shell: a general route to water soluble nanocrystals. *Nano Lett.*, 2004, **4(4):** 703–707.

[14] TORCHILIN V P, SHTILMAN M I, TRUBETSKOY V S, *et al*. Amphiphilic vinyl polymers effectively prolong liposome circulation time *in vivo*. *Biochimica et Biophysica Acta (BBA)-Biomembranes*, 1994, **1195(1):** 181–184.

[15] DENGLER E C, LIU J, KERWIN A, *et al*. Mesoporous silica-supported lipid bilayers (protocells) for DNA cargo delivery to the spinal cord. *J. Controlled Release*, 2013, **168(2):** 209–224.

[16] MELLAERTS R, FAYAD E J, VAN DEN MOOTER G, *et al*. *In Situ* FT-IR investigation of etravirine speciation in pores of SBA-15 ordered mesoporous silica material upon contact with water. *Mol. Pharmaceutics*, 2013, **10:** 567–573.

[17] CHEON J Y, AHN C, YOU D J, *et al*. Ordered mesoporous carbon-carbon nanotube nanocomposites as highly conductive and durable cathode catalyst supports for polymer electrolyte fuel cells. *J. Mater. Chem.*, 2013, **1(4):** 1270–1283.

[18] FANG Y, LV Y, CHE R, *et al*. Two-dimensional mesoporous carbon nanosheets and their derived graphene nanosheets: synthesis and efficient lithium ion storage. *J. Am. Chem. Soc.*, 2013, **135(4):** 1524–1530.

[19] CAI W, YU J, ANAND C, *et al*. Facile synthesis of ordered mesoporous alumina and alumina-supported metal oxides with tailored adsorption and framework properties. *Chem. Mater.*, 2011, **23(5):** 1147-1157.

[20] CHEN C, AHN W S. CO_2 capture using mesoporous alumina prepared by a Sol-Gel process. *Chem. Eng. J.*, 2011, **166(2):** 646–651.

[21] XU J, WANG A, WANG X, *et al*. Synthesis, characterization, and catalytic application of highly ordered mesoporous alumina-carbon nanocomposites. *Nano Research*, 2011, **4(1):** 50–60.

[22] HOUNSLOW M, MUMTAZ H, COLLIER A, *et al*. A micro-mechanical model for the rate of aggregation during precipitation from solution. *Chem. Eng. Sci.*, 2001, **56(7):** 2543–2552.

[23] CLARIDGE J B, YORK A P, BRUNGS A J, *et al*. Study of the temperature-programmed reaction synthesis of early transition metal carbide and nitride catalyst materials from oxide precursors. *Chem. Mater.*, 2000, **12(1):** 132–142.

[24] ZHAO Z, ZHANG W, REN P, *et al*. Insights into the topotactic conversion process from layered silicate RUB-36 to FER-type zeolite by layer reassembly. *Chem. Mater.*, 2013, **25(6):** 840–847.

[25] CUDENNEC Y, LECERF A. The transformation of Cu $(OH)_2$ into CuO, revisited. *Solid State Sciences*, 2003, **5(11):** 1471–1474.

[26] GOULD W, COOK F, WEBSTER G. Factors affecting urea hydrolysis in several Alberta soils. *Plant Soil*, 1973, **38(2):** 393–401.

[27] LIAO H D, ZHANG W P, SUN X M, *et al*. Preparation and thermodynamic study of self-dispersal nano-AlOOH. *Key Eng. Mater.*, 2012, **512:**100-105.

[28] BURTON W K, CABRERA N, FRANK F. The growth of crystals and the equilibrium structure of their surfaces. *Philos. Trans. R. Soc. A*, 1951, **243(866):** 299–358.

[29] PENN R L, BANFIELD J F. Morphology development and crystal growth in nanocrystalline aggregates under hydrothermal conditions: Insights from titania. *Geochim Cosmochim Acta*, 1999, **63(10):** 1549–1557.

[30] NAGAHAMA K, OUCHI T, OHYA Y. Temperature‐induced hydrogels through self-Assembly of cholesterol-substituted star PEG-b-PLLA copolymers: an injectable scaffold for tissue engineering. *Adv. Funct. Mater.*, 2008, **18(8):** 1220–1231.

[31] ZHI H, LÜ C, ZHANG Q, *et al*. A new PEG-1000-based dicationic ionic liquid exhibiting temperature-dependent phase behavior with toluene and its application in one-pot synthesis of benzopyrans. *Chem. Commun.*, 2009, **20:** 2878–2880.

[32] LI Y, PENG C, LI L, *et al*. Self-assembled 3D Hierarchically structured γ-alumina by hydrothermal method. *J. Am. Ceram. Soc.*, 2014, **97(1):** 35–39.

[33] YU Z Q, CHANG D, LI C, *et al*. Blue photoluminescent properties of pure nanostructured γ-Al_2O_3. *J. Mater. Res.*, 2001, **16(7):** 1890–1893.

水热法制备介孔氧化铝的形貌演化研究

李艳辉, 彭 诚, 赵 威, 白明敏, 饶平根

(华南理工大学 材料科学与工程学院, 广州 510640)

摘 要: 以硫酸铝铵、尿素为原料, PEG2000 作为分散剂, 通过水热法合成了三种形貌的勃姆石(AlOOH)。实验结果显示, 调节水热温度可以制备出 AlOOH 微球、微纤维和 3D 分级结构的 AlOOH。经 SEM 分析可知, 在煅烧过程中, AlOOH 分解转化为γ-Al_2O_3, 该过程为拓扑过程, 即形貌未发生变化。TEM 结果显示, 介孔均匀地分布在 AlOOH 内。基于此, 我们提出了温度–形貌生长机制。此外, 还研究了γ-Al_2O_3 的光致发光性能, 以 325 nm 为激发光谱时, 其发生光谱的波长在 380~500 nm, 光谱中心在 409 和 467 nm 处。

关 键 词: 勃姆石; γ-Al_2O_3; 拓扑; 介孔; 光致发光

中图分类号: TQ174 **文献标识码:** A